Water Research 290 (2026) 125096

Contents lists available at ScienceDirect

Water Research

journal homepage: www.elsevier.com/locate/watres

An N_2O emissions model featuring newly integrated abiotic pathways in nitrification

Wenbo Yu [a], Xiaodi Hao [a,*], Yuanyuan Wu [a], Mark C.M. van Loosdrecht [a,b]

[a] Sino-Dutch R&D Centre for Future Wastewater Treatment Technologies/Beijing Advanced Innovation Centre of Future Urban Design, Beijing University of Civil Engineering & Architecture, Beijing 100044, China
[b] Department of Biotechnology, Delft University of Technology, van der Maasweg 9, HZ, Delft 2629, the Netherlands

HIGHLIGHTS

- An existing nitrification model is enhanced by the integration of a key abiotic N_2O pathway.
- The model's predictions correlate well with observed data (49% vs. 51%).
- The model demonstrates efficiency in predicting partial nitrification + the Anammox system.
- The model's parameters remain robust under standard nitrification conditions with default values.

ARTICLE INFO

Keywords:
Nitrification
Sensitivity analysis
N_2O
Modeling
Abiotic pathway
Mitigation strategies

ABSTRACT

Nitrification in biological wastewater treatment is a significant source of nitrous oxide (N_2O), a potent greenhouse gas (GHG). There are some models that describe the biological N_2O production process, but they don't include abiotic N_2O production pathways which, remarkably, contribute up to 50% of the total N_2O emissions under high nitrite (NO_2^-) conditions. This limitation frequently results in pronounced predictive biases under high influent ammonium (NH_4^+) and intermediate NO_2^- conditions (such as in the partial nitrification + Anammox system), leading to the misidentification of N_2O emissions, undermining the development of effective mitigation strategies. To address this gap, a key abiotic N_2O production pathway was integrated into an existing model of nitrification which includes biological N_2O emissions. The upgraded model was systematically evaluated using literature-derived case studies, and can effectively predict the contributions of the abiotic pathway to N_2O emissions (49%), compared to experimental data (51%). A local sensitivity analysis confirms that the upgraded model has a resilience to perturbations within most parameters, although very high concentrations of NO_2^- (>1,000 mg N/L) necessitate a precise calibration of ammonium oxidation to nitrite (the AOB process), in which related parameters can more easily be measured in experiments. Moreover, a global sensitivity analysis demonstrates that dissolved oxygen (DO) and alkalinity are the most sensitive of the four key environmental factors (NH_4^+, NO_2^-, DO and alkalinity) which control N_2O emissions.

1. Introduction

The global average surface temperature has already risen by 1.59°C (IPCC, 2021), making the global warming a significant threat to human beings and ecology. For this reason, greenhouse gas (GHG) emissions must be substantially reduced, which has become a consensus and an urgent requirement for the international community (Schleussner et al., 2016). As a potent GHG among others, nitrous oxide (N_2O) has a global warming potential (GWP) 273 times higher than CO_2 and can persist in the atmosphere for 114 years (IPCC, 2021), thus constituting a serious threat to climate change.

The processes of wastewater treatment have been identified as a significant source of the N_2O emissions, which is generally considered to be the primary direct GHG emissions from wastewater treatment plants (WWTPs), accounting for about 80% of the direct GHG emissions (Longo et al., 2017). Wastewater treatment globally generates 2-5 million tons N_2O-N (equivalent to 858-2,145 million tons $CO_{2\text{-eq}}$) per year, accounting for 7.9%-11.4% of the total N_2O emissions from human

* Corresponding author.
E-mail address: xdhao@hotmail.com (X. Hao).

https://doi.org/10.1016/j.watres.2025.125096
Received 11 September 2025; Received in revised form 10 November 2025; Accepted 2 December 2025
Available online 4 December 2025

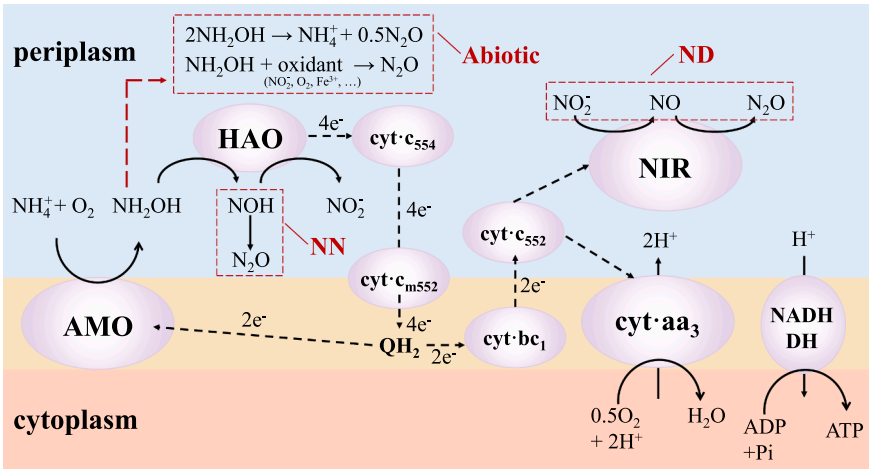

Fig. 1. Nitritation process of ammonia-oxidizing bacteria (AOB).

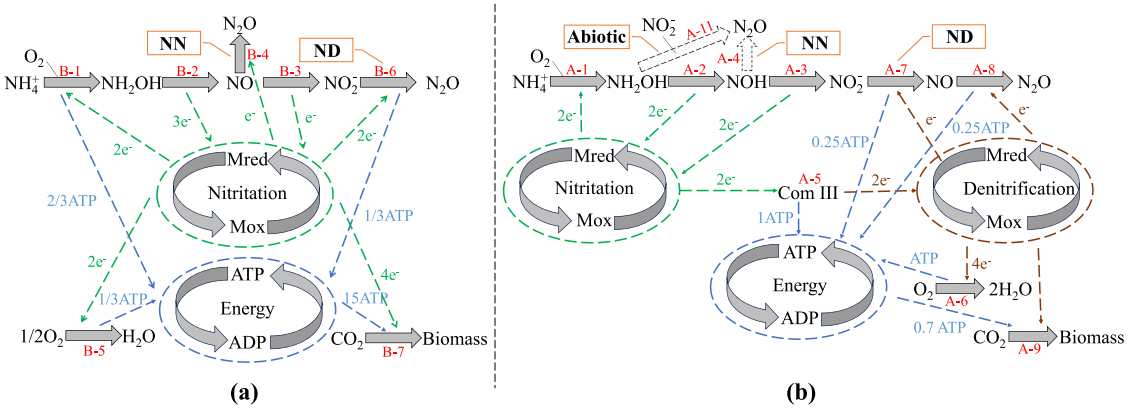

Fig. 2. Structure of the original model (a); the upgraded model (b).

activities (IPCC, 2021; Lu et al., 2018). Therefore, controlling the N_2O emissions from WWTPs is an urgent strategy.

During wastewater treatment, N_2O is primarily generated in both nitrification and denitrification processes. The nitritation process dominated by ammonia-oxidizing bacteria (AOB) contributes to the majority of the total N_2O emissions, while the nitratation process dominated by nitrite-oxidizing bacteria (NOB) does not produce N_2O (Wunderlin et al., 2012). As illustrated in Fig. 1, AOB produce N_2O via three main pathways (Chen et al., 2020; Vasilaki et al., 2019): 1) nitrifier denitrification (ND) pathway, where AOB utilize NO_2^- as an electron acceptor, reducing it to N_2O; 2) nitrifier nitrification (NN) pathway, involving the incomplete oxidation of intermediate metabolites NH_2OH, leading to N_2O release; 3) abiotic pathways, i) NH_2OH reacts chemically with NO_2^-, O_2, and/or other oxidants, or ii) disproportionation of NH_2OH to produce N_2O. In the abiotic pathways, the oxidation of NH_2OH by NO_2^- is a key reaction, as its rate exhibits 1-3 orders of magnitude higher than those of other reactions (Su et al., 2019). Although the ND and NN pathways seem to dominate the N_2O emissions in a typical nitrification system (Harris et al., 2015; Khalil et al., 2023), some studies have found that in reactors with high NO_2^- concentrations (such as the Sharon process) the significance of the abiotic pathways increases substantially, contributing to up to 50% of the N_2O emissions (Soler-Jofra et al., 2016; Terada et al., 2017).

On the other hand, existing predictive models for the nitrification-derived N_2O emissions ignored the abiotic pathways, only focusing primarily on the ND and NN ones. This limitation has significantly restricted their predictive accuracy in high-NO_2^- reactors such as nitritation + Anammox, nowadays enthused) and hindered their practicality on process optimization and N_2O emissions control. The ASM2d-N_2O model was extended from the ASM2d framework by incorporating the N_2O emissions from nitrification and denitrification, which comprehensively describes the entire wastewater biotreatment process with 24 components and 38 biological processes (Pocquet et al., 2016; Solís et al., 2022), but the nitrification module in this model only includes the ND and NN pathways, designating NH_2OH as the key substrate driving the N_2O production. Some studies have confirmed that ASM2d-N_2O performs poorly in predicting N_2O emissions under high-NO_2^- conditions (Mampaey et al., 2019). Peng et al. (2016) proposed a nitrification model coupling microbial metabolism through electron and energy carriers, providing a complete quantitative description of the ND and NN pathways' kinetics., but the abiotic pathways were not included yet.

To address the gap, this study introduces a key abiotic N_2O production pathway (the oxidation of NH_2OH by NO_2^-) to the model of Peng et al. (2016), alongside structural refinements and optimizations to enhance the prediction accuracy and to expand applicability. Three practical scenarios from the existing literature were selected to verify the upgraded model. The upgraded model can get a good predictive match (49%) up with the experimental data (51%) in the N_2O emissions from the abiotic passway (Terada et al., 2017). Subsequently, a local sensitivity analysis was performed to identify the influential intensity of key model parameters, providing a theoretical basis for model parameter calibration. Finally, a global sensitivity analysis was conducted to systematically evaluate the individual and synergistic effects of four critical environmental factors, dissolved oxygen (DO), NH_4^+, NO_2^- and alkalinity, on the model-predicted N_2O emissions. The study aims to offer a theoretical support on developing N_2O mitigation strategies in

Table 1
Stoichiometric matrix and composition matrix of the upgraded model.

Process		$S_{NH_4^+}$	S_{NH_2OH}	S_{NOH}	$S_{NO_2^-}$	S_{NO}	S_{N_2O}	S_{O_2}	S_{ALK}	S_{IC}	$S^{AOB}_{Mred\_N}$	$S^{AOB}_{Mred\_DN}$	S^{AOB}_{ATP}	X_{AOB}
A-1	$NH_4^+ \rightarrow NH_2OH$	-14	14					-32	1		-1			
A-2	$NH_2OH \rightarrow NOH$		-14	14					-2		1			
A-3	$NOH \rightarrow NO_2^-$			-14	14				-3		1			
A-4	$NOH \rightarrow N_2O$			-1			1							
A-5	Electron transportation										-1	1	1	
A-6	O_2 reduction							-16	2			-1	0.5	
A-7	$NO_2^- \rightarrow NO$				-14	14			2			-0.5	0.25	
A-8	$NO \rightarrow N_2O$					-14	14		1			-0.5	0.25	
A-9	AOBs growth	$-i_{NBM}$								-0.031		-0.062	-0.474	1
A-10	AOBs decay	i_{NBM}									0.0125			-1
A-11	NH_2OH abiotic oxidation		-0.5		-0.5		1							

Table 2
Process rates of the upgraded model.

Process	Rate
A-1	$\mu^{AOB}_{NH_4,ox}\frac{S_{O_2}}{S_{O_2}+K^{AOB}_{O_2,ox}}\frac{S_{NH_4^+}}{S_{NH_4^+}+K^{AOB}_{NH_4^+}+K^{AOB}_{I,FA}}\frac{f^{AOB}_{Mred\_N}}{f^{AOB}_{Mred\_N}+K^{AOB}_{Mred\_N,1}}\frac{K^{AOB}_{I,NH_2OH}}{K^{AOB}_{I,NH_2OH}+S_{NH_2OH}}X_{AOB}\cdot C^{AOB}_T$
A-2	$\mu^{AOB}_{NH_2OH,ox}\frac{S_{NH_2OH}}{S_{NH_2OH}+K^{AOB}_{NH_2OH}}\frac{f^{AOB}_{Mred\_N,max}-f^{AOB}_{Mred\_N}}{f^{AOB}_{Mred\_N,max}-f^{AOB}_{Mred\_N}+K^{AOB}_{Mox,N}}\frac{S_{ALK}}{S_{ALK}+K^{AOB}_{ALK,1}}X_{AOB}\cdot C^{AOB}_T$
A-3	$\mu^{AOB}_{NOH,ox}\frac{S_{NOH}}{S_{NOH}+K^{AOB}_{NOH}}\frac{f^{AOB}_{Mred\_N,max}-f^{AOB}_{Mred\_N}}{f^{AOB}_{Mred\_N,max}-f^{AOB}_{Mred\_N}+K^{AOB}_{Mox,N}}\frac{S_{ALK}}{S_{ALK}+K^{AOB}_{ALK,2}}X_{AOB}\cdot C^{AOB}_T$
A-4	$\mu^{Che}_{NOH,deg}\cdot(S_{NOH})^2$
A-5	$\mu^{AOB}_{ComIII}\frac{f^{AOB}_{Mred\_N}}{f^{AOB}_{Mred\_N}+K^{AOB}_{Mred\_N,2}}\frac{f^{AOB}_{Mred\_DN,max}-f^{AOB}_{Mred\_DN}}{f^{AOB}_{Mred\_DN,max}-f^{AOB}_{Mred\_DN}+K^{AOB}_{Mox\_DN}}\frac{f^{AOB}_{ATP,max}-f^{AOB}_{ATP}}{f^{AOB}_{ATP,max}-f^{AOB}_{ATP}+K^{AOB}_{ADP}}X_{AOB}\cdot C^{AOB}_T$
A-6	$\mu^{AOB}_{O_2,red}\frac{S_{O_2}}{S_{O_2}+K^{AOB}_{O_2,red}}\frac{f^{AOB}_{Mred\_DN}}{f^{AOB}_{Mred\_DN}+K^{AOB}_{Mred\_DN,1}}\frac{f^{AOB}_{ATP,max}-f^{AOB}_{ATP}}{f^{AOB}_{ATP,max}-f^{AOB}_{ATP}+K^{AOB}_{ADP}}X_{AOB}\cdot C^{AOB}_T$
A-7	$\mu^{AOB}_{NO_2,red}\frac{S_{NO_2^-}}{S_{NO_2^-}+K^{AOB}_{NO_2,red}+K^{AOB}_{I,FNA}}\frac{f^{AOB}_{Mred\_DN}}{f^{AOB}_{Mred\_DN}+K^{AOB}_{Mred\_DN,2}}\frac{f^{AOB}_{ATP,max}-f^{AOB}_{ATP}}{f^{AOB}_{ATP,max}-f^{AOB}_{ATP}+K^{AOB}_{ADP}}X_{AOB}\cdot C^{AOB}_T$
A-8	$\mu^{AOB}_{NO,red}\frac{S_{NO}}{S_{NO}+K^{AOB}_{NO,red}}\frac{f^{AOB}_{Mred\_DN}}{f^{AOB}_{Mred\_DN}+K^{AOB}_{Mred\_DN,3}}\frac{f^{AOB}_{ATP,max}-f^{AOB}_{ATP}}{f^{AOB}_{ATP,max}-f^{AOB}_{ATP}+K^{AOB}_{ADP}}X_{AOB}\cdot C^{AOB}_T$
A-9	$\mu^{AOB}_{growth}\frac{S_{IC}}{S_{IC}+K^{AOB}_{IC}}\frac{f^{AOB}_{Mred\_DN}}{f^{AOB}_{Mred\_DN}+K^{AOB}_{Mred\_DN,4}\cdot X_{AOB}}\frac{f^{AOB}_{ATP}}{f^{AOB}_{ATP}+K^{AOB}_{ATP}}M_{NH4}\cdot M_{NPO4}\cdot X_{AOB}\cdot C^{AOB}_T$
A-10	$b_{AOB}\cdot X_{AOB}\cdot C^{AOB}_T$
A-11	$\mu^{Che}_{NH_2OH,NO2}\cdot S_{NH_2OH}\cdot S_{NO_2^-}$

the process of nitrification.

2. Modeling methodology

2.1. Model Structure

The upgraded model is based on the original model proposed by Peng et al. (2016). The model structure is illustrated in Fig. 2. The stoichiometric matrix and process kinetics of the upgraded model are presented in Tables 1 and 2, respectively. The matrices, kinetic rates of the original model, and parameters of both models are provided in the Supplementary Materials.

The upgraded model includes all three N_2O production pathways:

1) the NN pathway (Reactions A-2 and A-3): Nitroxyl (NOH) is utilized as the intermediate for nitritation (Duan et al., 2017). Its chemical degradation (Reaction A-4) is designated as the NN pathway for the N_2O production. Some previous models adopting NOH employed the first-order kinetics for degradation (Law et al., 2012; Lv et al., 2022; Ni and Yuan, 2015), which misrepresented the actual chemical reaction dynamics. Although the model structure is simplified, the first-order kinetics might yield significant deviations in simulating NOH. Here, Reaction A-4 follows the second-order kinetics to better reflect some real processes. However, validation remains a challenge due to some current limitations in NOH quantification (Schreiber et al., 2012).
2) the ND pathway (Reactions A-7 and A-8): NO_2^- is utilized as electron acceptors to generate ATP and N_2O. Therefore, O_2 and NO_2^- compete for reductive substrates, and the N_2O production surges substantially under a low DO.
3) the abiotic pathway (Reaction A-11) involves the chemical reaction of NH_2OH. N_2O is generated through the reactions of NH_2OH with oxidants (e.g., NO_2^-, O_2, Fe^{3+}, etc.) or NH_2OH disproportionation. However, some previous studies confirmed that the NH_2OH/NO_2^- reaction dominated the abiotic N_2O generation in typical wastewater systems, with its rate being 1-3 orders of magnitude higher than other reactions (Soler-Jofra et al., 2016; Su et al., 2019). Thus, only Reaction A-11 is included to represent the abiotic N_2O production.

Simultaneously, the structure and parameters of the original model were revised and optimized. The electron carrier pool was partitioned into two distinct pools in the upgraded model, involving the processes of AOB ($NH_4^+ \rightarrow NO_2^-$) and denitrification ($NO_2^- \rightarrow N_2O$) respectively. This modification better reflects the actual microbial processes and corrects an issue in the original model where the ammonia oxidation rate (Reaction A-1) is influenced due to a substrate competition with respiratory reactions (Reactions A-6 to A-8). Electrons generated from nitritation are transferred to the denitrification pool via Complex III while producing ATP (Reaction A-5). Given the higher redox potential in the nitritation pool, this reaction is unidirectional (no reverse flow). Furthermore, inhibition terms were incorporated into the original model, extending the applicability of the upgraded model. Based on the evidence that free ammonia (FA) (Ding et al., 2016) and its intermediate

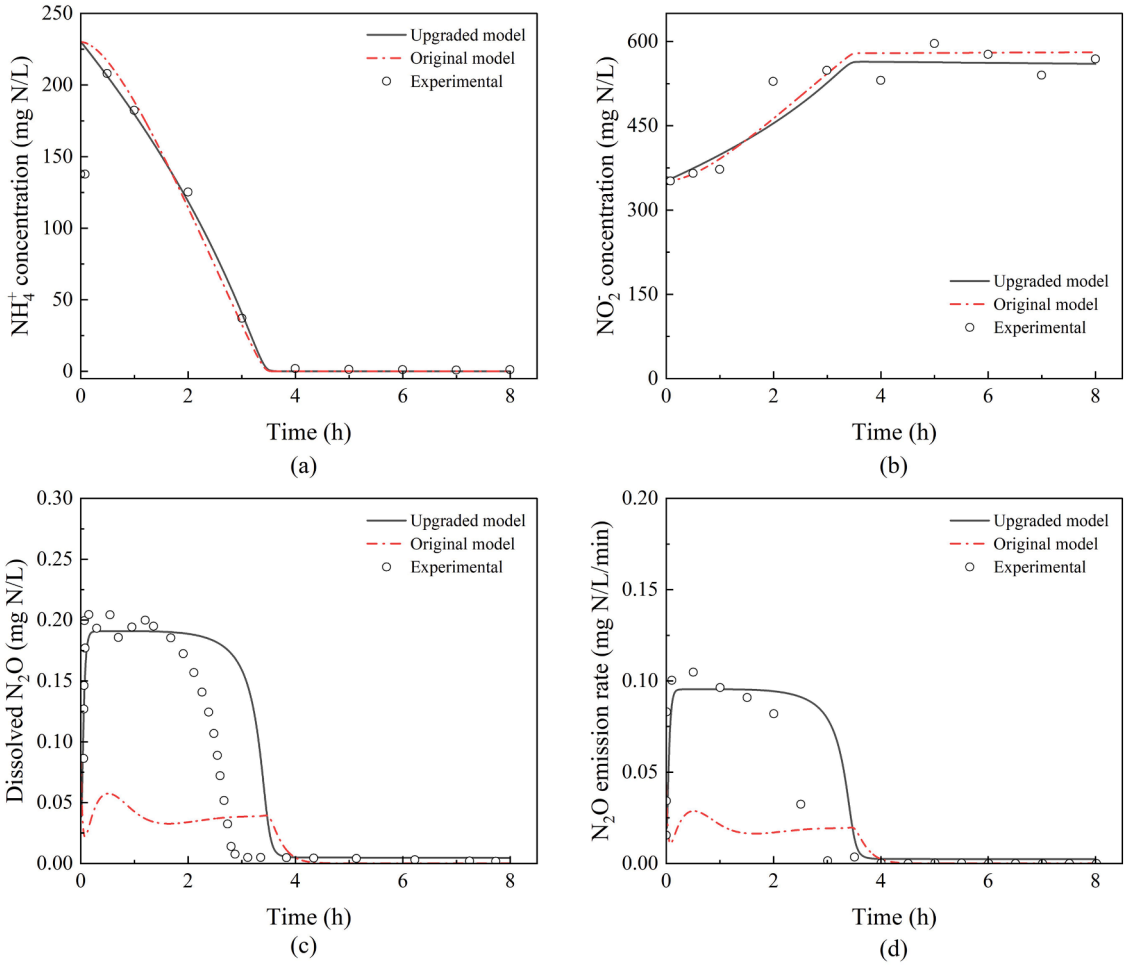

Fig. 3. Simulation results of the two models, based on Scenario A: NH_4^+ (a); NO_2^- (b); dissolved N_2O (c); gaseous N_2O emissions rate (d).

Table 3
Model validation error metrics.

	The upgraded model		The original model	
	RMSE (mg N·L^{-1}·min^{-1})	MAPE (%)	RMSE (mg N·L^{-1}·min^{-1})	MAPE (%)
Scenario A (0.8 h shifted, 2.5 h-7 h)	0.00057	8.8	0.035	75.6
Scenario B	0.0146	38.3	0.036	52.0
Scenario C	0.0036	26.1	0.00802	1832

NH_2OH (Zhao et al., 2022) inhibit this reaction due to toxic effects. Therefore, a competitive inhibition by FA and a non-competitive inhibition by NH_2OH were added to the kinetics. These terms also serve as the microbial feedback mechanisms under unfavorable conditions. Meanwhile, NH_2OH inhibition of nitrite oxidizing bacteria (NOB) (Zhao et al., 2022) was implemented by increasing the saturation coefficient (without altering maximum rates) in the NOB nitrification kinetics. Moreover, microbial decay (Reaction A-10) releases electrons into the nitritation pool, simulating endogenous respiration.

2.2. Experimental data

Three different experimental datasets were utilized to calibrate and validate the model:

1) Scenario A, a high NO_2^- accumulation in nitritation (Terada et al., 2017). A lab-scale SBR system with a working volume of 1 L was employed. The operational conditions included MLVSS= 1720 ± 70 mg/L, a controlled temperature of 28°C, and an aeration rate of 1 L/min. Alkalinity was automatically dosed into the reactors to maintain pH at 7.0. Thus, alkalinity was considered to be sufficient enough in modeling. Real-time monitoring tracked the dynamic changes in the concentrations of NH_4^+, NO_2^- NO_3^- and N_2O. The initial NH_4^+ (^{15}N-labeled) and NO_2^- concentrations were 200 and 400 mg-N/L, respectively. The contributions of individual pathways to the N_2O production were determined through the isotopic analysis of the emitted N_2O.
2) Scenario B, full nitrification limited by inorganic carbon source (Peng et al., 2015). A lab-scale SBR (1 L working volume) with MLVSS=222 mg/L was utilized. The operational parameters encompassed a temperature range of 22–23°C, aeration rate= 0.5 L/min, and DO= 2.5 mg O_2/L. Alkalinity was automatically dosed to the reactors to maintain pH at 7.5. Thus, the alkalinity is considered to be sufficient enough in modeling. The concentrations of NH_4^+, NO_2^-, NO_3^- and N_2O were continuously monitored. To maintain a constant NH_4^+ level of 20 mg-N/L, periodic substrate additions were performed every 20 min. The initial inorganic carbon (IC) concentration was approximately 12.5 mmol C/L. Continuous aeration gradually stripped IC (as CO_2), inducing a progressive decline in IC concentration and establishing carbon-limited conditions.
3) Scenario C, a high-NH_4^+ Sharon process (Kampschreur et al., 2008; Soler-Jofra et al., 2016). A full-scale Sharon process at a plant received ammonium-rich reject water derived from anaerobic

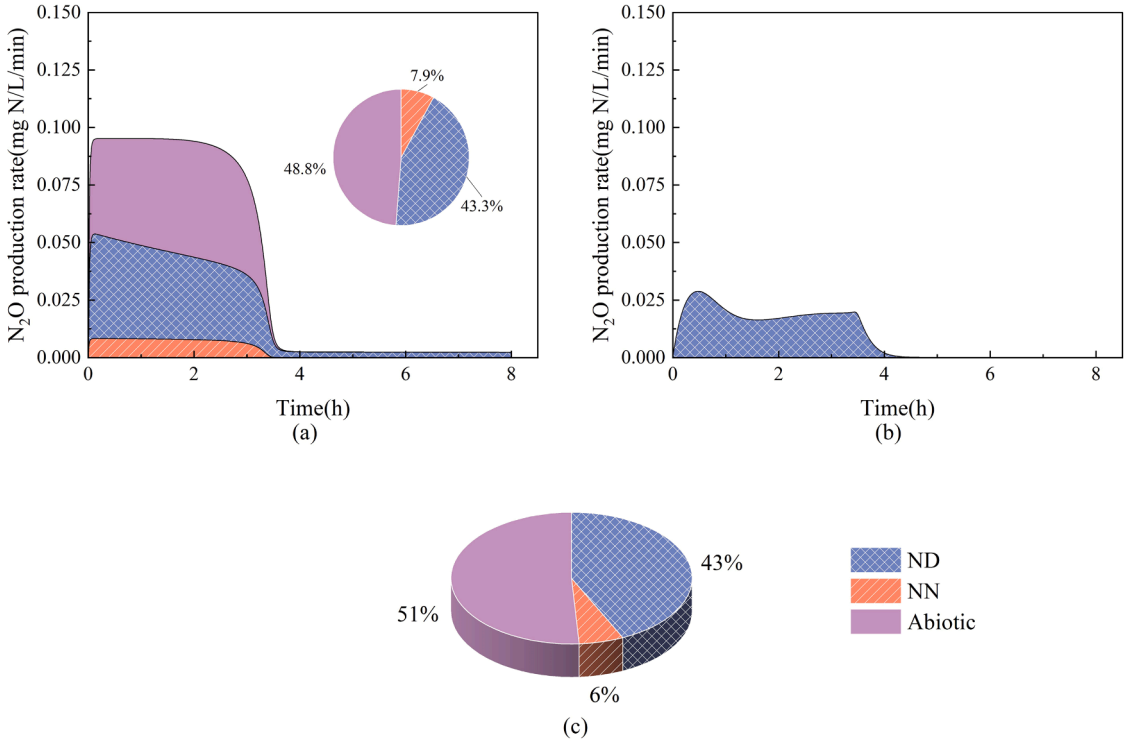

Fig. 4. Proportional contributions of the N_2O production pathways from the upgraded model (a); the original model (b); experimental data (c).

digestion of waste sludge, where approximately 55% of the influent NH_4^+ was oxidized to NO_2^- within the Sharon reactor. The effluent was subsequently treated in an Anammox reactor for further nitrogen removal. Monitoring occurred between January and June 2006. The reactor volume was 1,500 m^3, with an average flow rate of 600 m^3/d and an average influent NH_4^+ concentration of 1,400 mg N/L. The operational cycle consisted of aeration for 90 min, followed by 30 min non-aeration (the total cycle for 2 h). The key monitored parameters included the dynamic concentrations of NH_2OH, NO, and N_2O. Additionally, the NO and N_2O concentrations would undergo a detailed real-time monitoring over a defined period.

2.3. Modelling methodology

A software, Aquasim 2.1, was applied to implement model construction, parameter calibration, and simulation. The upgraded model and the original model were employed to simulate the same experimental data from the three scenarios for systematically evaluating their accuracy and practicality in describing the nitrogen transformation and N_2O production processes.

2.4. Sensitivity analysis

2.4.1. Local sensitivity analysis

A local sensitivity analysis was conducted for all the parameters used in the upgraded model. The parameters were perturbed by ±5% from the baseline values with a standard deviation of 1%. Based on the data from the three scenarios, the N_2O production rate was served as a key output variable. The fluctuation range of this output induced by individual parameter perturbations was quantified. The composite sensitivity factor (SF) was calculated for each parameter according to Eq. 1:

$$SF = \frac{(A_{up} - A_{low})/A_{baseline}}{(F_{up} - F_{low})/F_{baseline}} \quad (1)$$

Where: SF, the composite sensitivity factor; A_{up} and A_{low}, the upper and lower bounds of output fluctuation, respectively; $A_{baseline}$, the baseline output value; F_{up} and F_{low}, the upper and lower perturbation bounds of the parameters; and $F_{baseline}$, the baseline parameters value. Parameters were classified into four categories based on SF magnitude: insensitive ($SF < 0.1$), moderately sensitive ($0.1 \leq SF < 0.5$), sensitive ($0.5 \leq SF < 1$), and highly sensitive ($SF \geq 1$).

2.4.2. Global sensitivity analysis

A global sensitivity analysis employing the Morris screening method was performed on the upgraded model to ascertain the influence of operational conditions on predicting the N_2O emissions factor (EF). The analyzed key variables included DO, NH_4^+, NO_2^-, and alkalinity (ALK) (Chen et al., 2020). Latin Hypercube Sampling generated a uniformly distributed baseline point set. Subsequently, 100 independent trajectories were created by randomly perturbing baseline points using Python. The upgraded model was executed for all the baseline and perturbed points to compute corresponding EF values, defined as:

$$EF = \frac{r_{N_2O}}{r_{NH_4ox}} \quad (2)$$

Where: r_{N2O}, the N_2O production rate (mg N/L/min); r_{NH4ox}, the NH_4^+ oxidation rate (mg N/L/min). The elementary effect (EE) for each parameter was calculated as:

$$EE = \frac{EF_i - EF}{\Delta_i} \quad (3)$$

Where: $EF_{baseline}$ and EF_i, emissions factors at the baseline and perturbed conditions, respectively; Δ_i, the parameter perturbation step size. The mean (μ*) and standard deviation (σ) of elementary effects across all the trajectories were computed to quantify overall parameter influence strength and nonlinear/interactive effects.

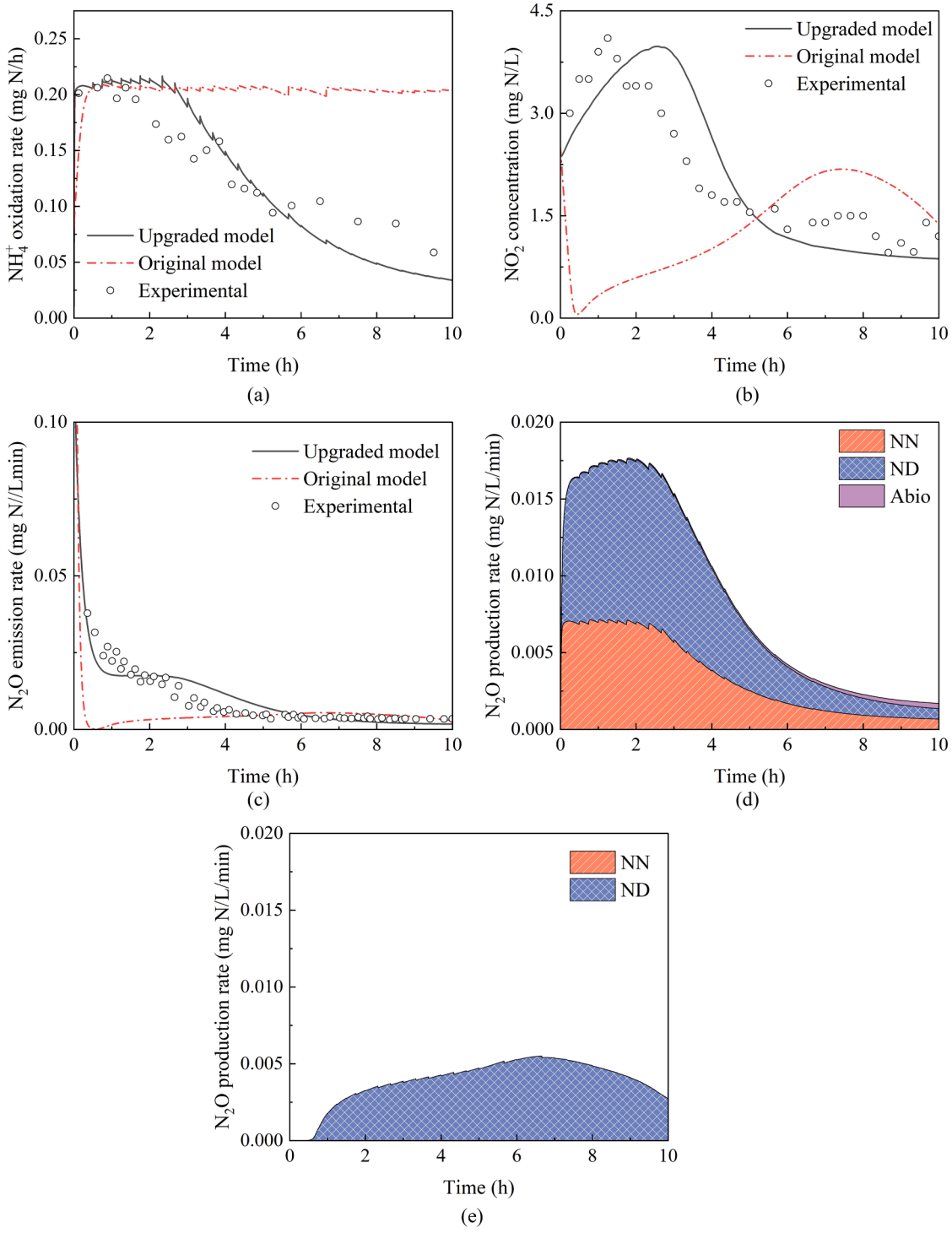

Fig. 5. Simulation results on Scenario B from two models: NH_4^+ oxidation rate (a); NO_2^- (b); N_2O emissions rate (c); proportional contributions of the N_2O production pathways predicted by the upgraded model (d) and by the original model (e).

3. Results and discussion

3.1. Simulation comparison by the two models

3.1.1. Scenario A

Based on Scenario A, the simulation results from the two models are shown in Fig. 3. Both models can effectively capture the dynamics of the NH_4^+ conversion to NO_2^- (Figs. 3a and 3b). However, the original model significantly underestimates both dissolved N_2O concentration (Fig. 3c) and N_2O emissions rate (Fig. 3d), whereas the upgraded model performs better. The simulated duration of the N_2O production process by the models is 0.8 hrs longer than that of the experimental data. However, the experimental data indicates that nearly 40 mg N/L of NH_4^+ remained in the reactor when the N_2O emissions had almost completely ceased. Therefore, the longer simulated N_2O emissions duration seems reasonable. Despite of this temporal discrepancy, the simulation curve of the upgraded model exhibits remarkably its similar dynamic characteristics on the experimental data. The peak height (experimental data: 0.105 mg

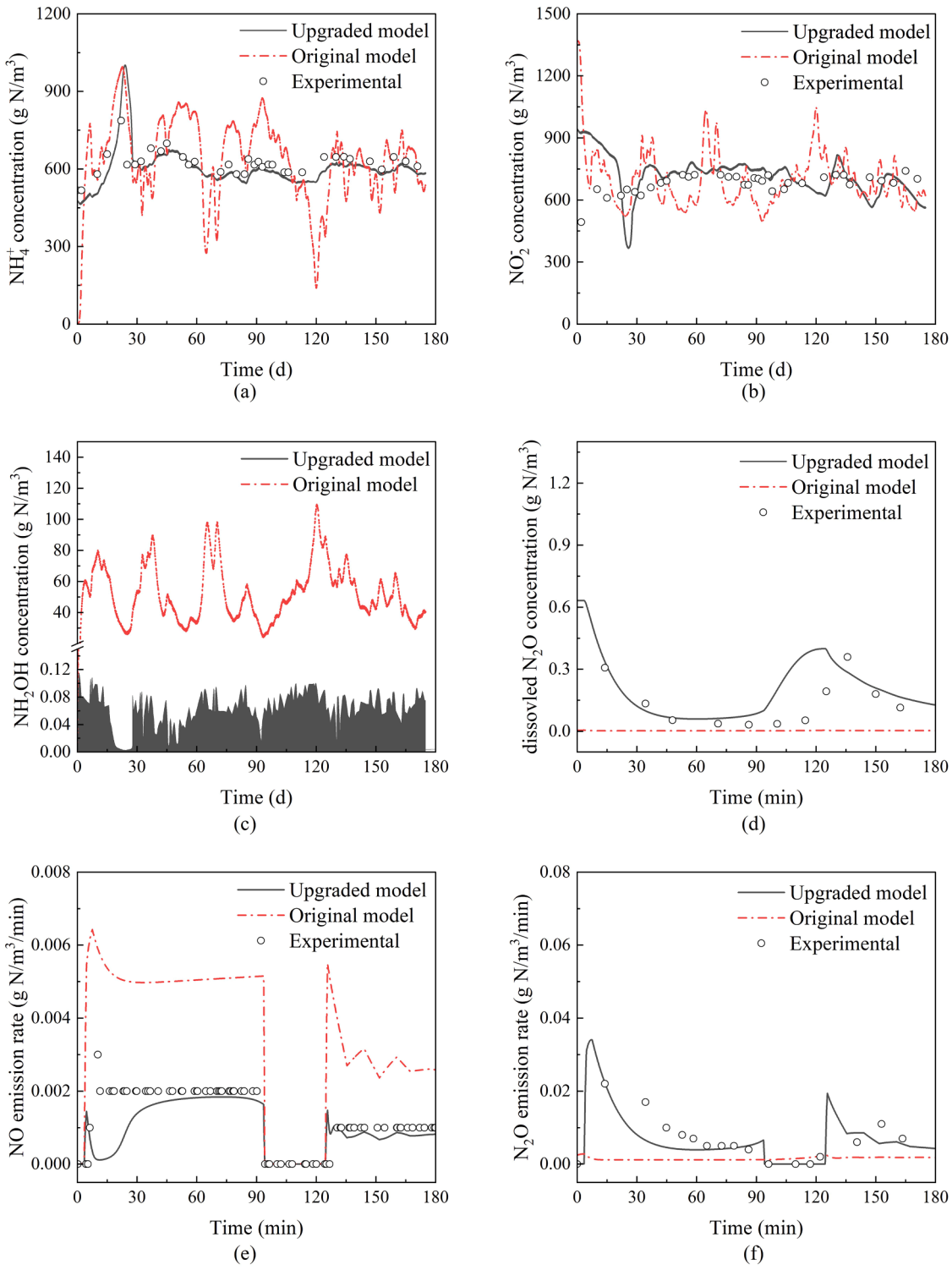

Fig. 6. Simulation results on Scenario C from the two models: NH_4^+ (a); NO_2^- (b); NH_2OH (c); dissolved N_2O (d); NO emissions rate (e); N_2O emission rate (f).

N/L/min, the upgraded model: 0.095 mg N/L/min) and the duration of declining phase (experimental data: 1.5 h, the upgraded model: 1.37 h) are basically consistent. Thus, that the upgraded model can effectively fit the N_2O production profile.

The results of root mean square error (RMSE) and mean absolute percentage error on simulating N_2O emissions rate are shown in Table 3. After applying a 0.8-hrs phase correction, the RMSE value from the upgraded model simulations dramatically decreases by 98.4% and MAPE improves from 75.6% to 8.8% (88.4% reduction), compared to the original model. The upgraded model effectively reduces errors, providing a reliable tool for the N_2O emissions prediction and reduction.

The proportional contributions of the N_2O production pathways are shown in Fig. 4. The ^{15}N isotope tracing technique revealed the proportional contributions of each pathway (Fig. 4c): the abiotic pathway accounted for up to 51% of the total N_2O production, while the ND pathway contributed 43%, which highlights the significance of the abiotic pathway in this case study. The result of the upgraded model aligns with the experimental data, validating the mechanistic rationale

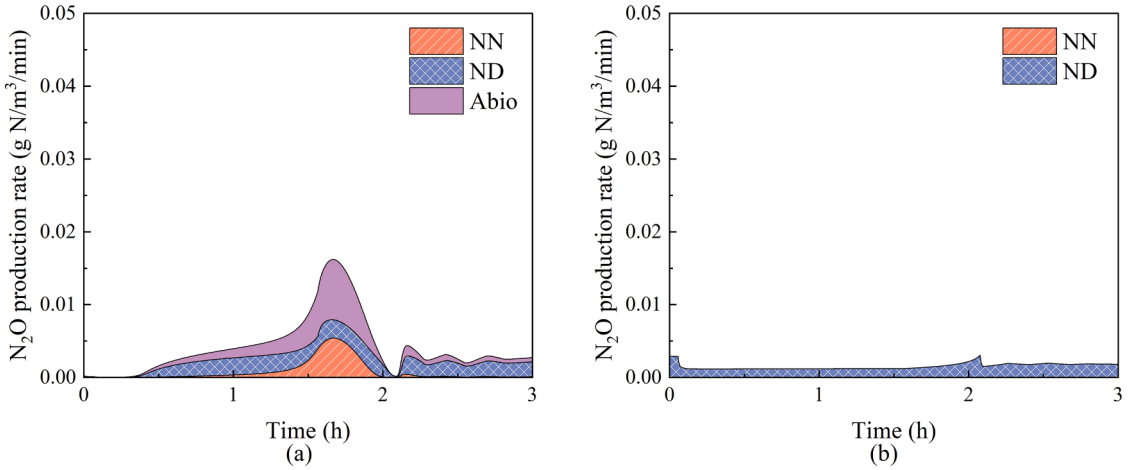

Fig. 7. Proportional contributions of N_2O production pathways of the upgraded model (a) and the original model (b).

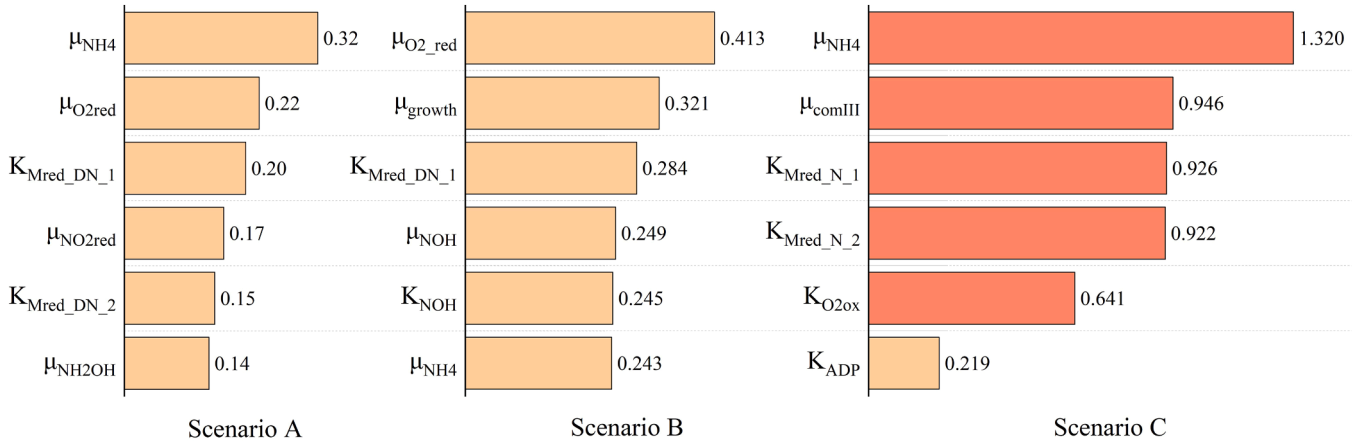

Fig. 8. Results of the local sensitivity analysis.

of the model. In contrast, the original model does not incorporate the abiotic pathway, and leads to a significant deviation in its predictions.

3.1.2. *Scenario B*

The simulation results on Scenario B from the two models are as shown as Fig. 5. Continuous aeration progressively stripped dissolved IC, which reduced from 12.5 mmol C/L to 0.4 mmol C/L. The upgraded model successfully captures the gradual inhibition of nitrification due to the IC scarcity: declined IC concentration slows AOB proliferation, triggering ATP accumulation and consequent activation of the negative feedback regulation mechanisms. This ultimately induces a significant NH_2OH accumulation (peak: 1.65 mg N/L), inhibiting NH_4^+ oxidation. Concurrently, elevated NH_2OH suppresses the NOB activity. The model-predicted dynamics of NH_4^+, NO_2^-, and N_2O align with the experimental measurements, confirming the efficacy of the metabolic feedback mechanisms under the IC-limiting conditions.

The original model also includes the influence of IC limitation, where the IC scarcity causes ATP accumulation to directly inhibit the process rate of NH_4^+ oxidation and respiration. Due to its reliance on a single electron carrier pool, however, the interactions between reactions are misrepresented, which leads the inhibition of respiration paradoxically promotes the NH_4^+ oxidation rate. Consequently, no significant inhibitory response in the NH_4^+ oxidation rate is observed within the simulation timeframe. The upgraded model demonstrates the enhanced performances (Table 3), with RMSE reduced from 0.036 to 0.0146 (59.4% reduction) and MAPE reduced from 52% to 38.3% (26.3% reduction).

The pathway contributions to the N_2O production in the two models are shown in Figs. 5d and 5e. In the upgraded model, the ND pathway accounts for 58.6% of the N_2O emissions, while the NN pathway contributes to 39.6%. Despite of a high NH_2OH concentration, the NO_2^- scarcity minimizes the abiotic pathway's contribution (1.8%). In contrast, the original model makes nearly all the N_2O production to the ND pathway.

3.1.3. *Scenario C*

The simulation results on Scenario C from the models are presented in Fig. 6. Insufficient influent alkalinity constrained the NH_4^+ conversion. The upgraded model can accurately simulate the dynamics of NH_4^+ and NO_2^- (Figs. 6a and 6b) by incorporating the alkalinity limitation mechanisms for the NH_2OH and NOH oxidation during nitritation. The original model neglected the influences of both alkalinity and pH, resulting in an overestimated NH_4^+ conversion.

The simulated NH_2OH concentrations are shown in Fig. 6c. The monitored data indicated the NH_2OH level in the reactor at 0.03–0.11 mg N/L (mean: 0.06 mg N/L) (Soler-Jofra et al., 2016). The upgraded model can simulate comparable results (0.003–0.115 mg N/L; mean: 0.045 mg N/L). In contrast, the original model treats NH_2OH as a theoretical intermediate without accounting for the abiotic consumption pathway, producing a significant deviation: the original model generates a physiologically implausible level (52.1 mg N/L). The superior NH_2OH prediction capability from the upgraded model substantiates the

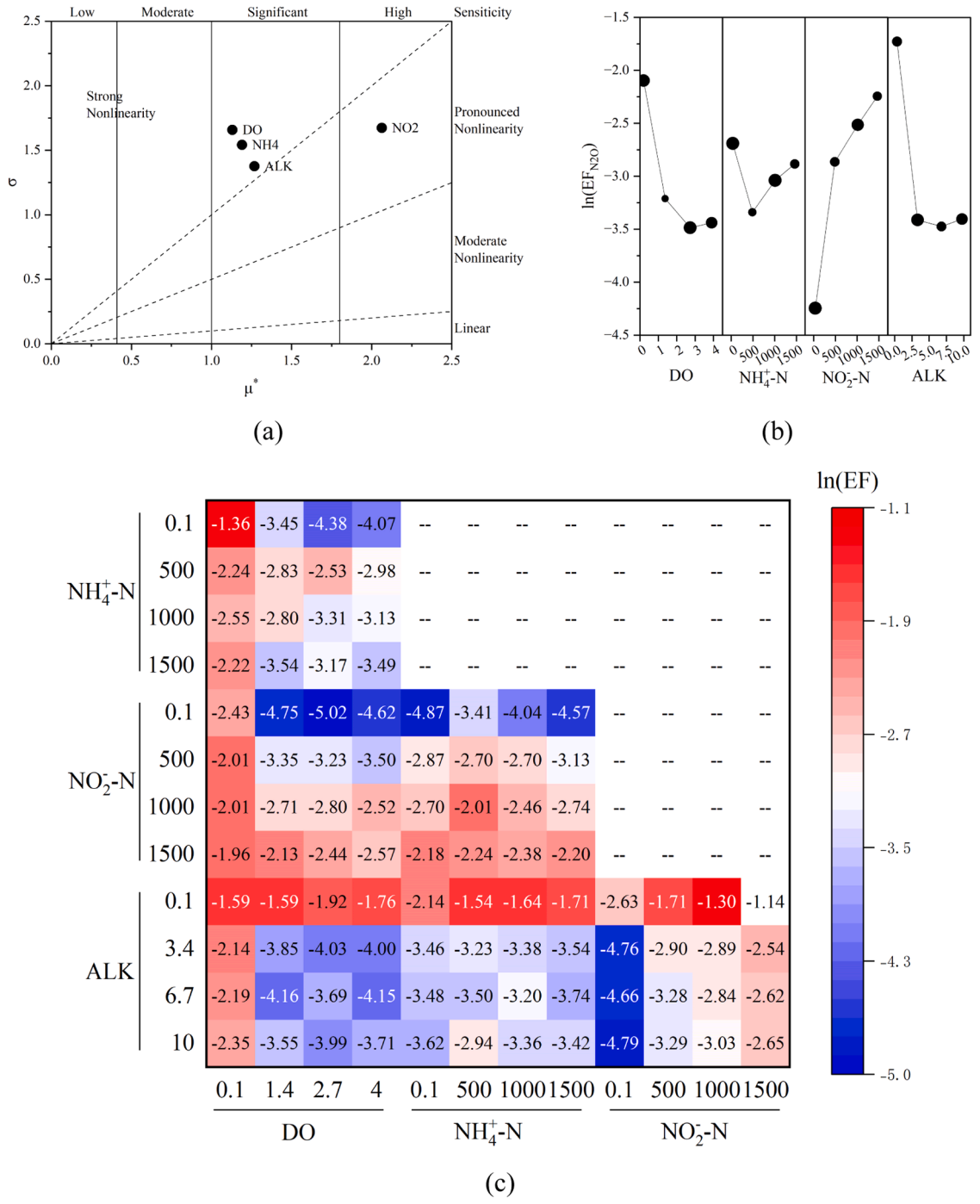

Fig. 9. Results of the Morris sensitivity analysis: μ*-σ diagnostics (a); elementary effect distribution (b); interaction heatmap (c).

reliability of its abiotic N_2O production pathway.

During the long-term operation, the measured average N_2O emissions rate was 0.47 g N/m^3/h. The upgraded model can closely fit this value (0.41 g N/m^3/h). For the selected operational periods (Figs. 6d-6f), the upgraded model demonstrates a strong agreement with the monitored data, yielding RMSE= 0.0036 mg-N/L and MAPE= 26.1% on the N_2O emissions rate (Table 3). The original model completely fails in simulating the N_2O production rate, with some critical errors (RMSE = 0.00802 and MAPE = 1832%)., which demonstrates the original model is not applicable to a high-NO_2^- environment. Conversely, the upgraded model can achieve an 55.1% reduction in RMSE and a significant improvement in MAPE, compared to the original model.

Furthermore, the upgraded model can effectively simulate the NO emissions rates (Fig. 6e), confirming the validity of its mechanisms designating NO exclusively as a denitrification intermediate. Conversely, the original model treats NO as an intermediate in nitritation process, overpredicting the NO emissions by 2.5-fold relative to the actual value.

The pathway contributions to the N_2O production during the monitoring period are illustrated in Fig. 7. Elevated NO_2^- concentrations in the upgraded model suppressed the ND pathway while enhancing the abiotic contribution. Simultaneously, alkalinity constraint promotes the intermediate accumulation (e.g., NH_2OH), increasing the NN pathway contribution.

3.2. Sensitivity analysis

3.2.1. Local sensitivity analysis

The results of a local sensitivity analysis are presented in Fig. 8. Under the medium and low TN loads (Scenarios A and B), all the parameters exhibit a moderate sensitivity (0.1< SF< 0.5) or insensitive (SF< 0.1), which indicates a good model stability. The default parameter values can be directly adopted, resulting in significant savings in time and cost during the model application.

Under the elevated NH_4^+ loading conditions (Scenario C), the parameters governing μ_{NH4}, $K_{Mred\_N\_1}$, K_{O2ox}, μ_{ComIII} and $K_{Mred\_N\_2}$ reveal a high sensitivity (SF> 0.5), which indicates that NH_4^+ oxidation acts as the rate-limiting step in the upgraded model under a high-load scenario, where minor parameter deviations can significantly amplify prediction errors; this condition aligns with the previous research findings (Bae et al., 2021). Consequently, the rigorous calibration and validation of NH_4^+ oxidation kinetic parameters are imperative when applying the upgraded model to such reactors to ensure a prediction accuracy and reliability.

3.2.2. Global Sensitivity Analysis

The results of the Morris sensitivity analysis are shown in Fig. 9. All the investigated variables significantly influence the EF of N_2O. The NO_2^- concentration exhibits the highest mean elementary effects (μ*), exceeding that of the second-ranked parameter (alkalinity) by approximately 63%, thus classified as a highly sensitive parameter, which demonstrates that NO_2^- is a pivotal driver of EF, particularly in high NO_2^- reactors, such as the Sharon system, where elevated NO_2^- levels significantly enhance the N_2O emissions. Although DO and alkalinity demonstrate a lower average μ*, they display a localized high sensitivity at low concentrations: when DO concentration falls below 1.3 mg/L, or alkalinity drops under 2.5 mmol/L, EF can increase dramatically. Above these thresholds, their sensitivity diminishes markedly.

NH_4^+ can generally exert a stable influence on EF, although elevated loading can induce a gradual upward trend, potentially reflecting heightened alkalinity dependency by AOB that amplifies the N_2O production. NO_2^- shows a strong positive correlation with EF: with a weak effect below 36 mg N/L, but there is a strong influence above this threshold, due to the enhanced abiotic pathway activity. Although it is negligible in typical nitrification reactors, the impact of NO_2^- requires a careful management in a nitritation system.

The interaction heatmap (Fig. 9c) highlights the synergistic parameter effects. Alkalinity deficiency and suboptimal DO emerge as the primary priorities for intervention, as the improvements from other parameters cannot offset their promotion on EF, which reveals that maintaining an adequate DO level constitutes the most critical EF mitigation lever in typical nitrification reactors, followed by preventing alkalinity depletion. For nitritation reactors, a high NO_2^- concentration becomes an additional dominant sensitivity factor. The interaction results demonstrate a low NH_4^+/NO_2^- associated with a low DO, and a high NH_4^+/NO_2^- combined with a low ALK would further elevate EF, which corroborates that the DO optimization can deliver a superior EF reduction in nitritation, whereas alkalinity supplementation can be a more efficient way in high-load nitritation reactors.

To mitigate N_2O emissions, as illustrated in Fig. 9c, a hierarchical control strategy can be recommended. The primary measure should maintain sufficient alkalinity above 2.5 mmol/L, and too much increasing alkalinity can only provide a marginal benefit for emissions reduction. Subsequently, the DO level should be controlled, ideally around 2.7 mg O_2/L and never falls below 1.3 mg O_2/L. For reactors employing the partial nitrification + Anammox process, it is advised to maintain the NO_2^- concentration below 1,000 mg/L with the DO level kept between 1.4-2.7 mg O_2/L.

4. Conclusions

A key abiotic N_2O production pathway was involved into an existing model of nitrification with the biological N_2O production processes, which can effectively predict the N_2O emissions with high nitrogen loadings, as the conditions occurring in partial nitrification + Anammox.

1) By integrating the abiotic N_2O emissions pathway, the upgraded model can significantly improve its prediction accuracy, compared to the original model. In the scenarios with low to medium TN loads, the RMSE of the N_2O emissions rate decreases by 59.4%-98.4%, and the MAPE reduces by 26.3%-88.4%; Under high NH_4^+ and NO_2^- concentrations, where the original model fails and the upgraded model achieves RMSE= 0.0036 mg $N{\cdot}L^{-1}{\cdot}min^{-1}$ and MAPE= 26.1%, having a good predictive match up with the experimental data in the N_2O emissions from the abiotic passway (49% predicted vs. 51% measured).
2) The local sensitivity analysis demonstrates that the model is robust to perturbations of most parameters. However, the kinetics of ammonia oxidation are highly sensitive to elevated NH_4^+ loading, which requires an experimental calibration.
3) The global sensitivity analysis identifies the NO_2^- concentration as the primary driver of the N_2O emissions factor (the highest mean sensitivity). When NO_2^-> 36 mg N/L, it can activate the abiotic N_2O emissions pathway, increasing the emissions factor (EF).
4) Both low DO (< 1.3 mg O_2/L) and alkalinity (< 2.5 mmol/L) can synergistically elevate the N_2O emissions factor.

CRediT authorship contribution statement

Wenbo Yu: Writing – original draft, Validation, Software, Methodology, Investigation, Formal analysis, Data curation. **Xiaodi Hao:** Writing – review & editing, Supervision, Project administration, Funding acquisition, Conceptualization. **Yuanyuan Wu:** Visualization, Resources. **Mark C.M. van Loosdrecht:** Supervision.

Declaration of competing interest

The authors declare that they have no known competing financial interests or personal relationships that could have appeared to influence the work reported in this paper.

Acknowledgements

The study was financially supported by the National Natural Science Foundation of China (52170018).

Supplementary materials

Supplementary material associated with this article can be found, in the online version, at doi:10.1016/j.watres.2025.125096.

Data availability

Data will be made available on request.

References

Bae, W.B, Park, Y., Chandran, K., Shin, J., Kang, S.B., Wang, J., Kim, Y.M., 2021. Temporal triggers of N_2O emissions during cyclical and seasonal variations of a full-scale sequencing batch reactor treating municipal wastewater. Sci. Total Environ. 797, 149093. https://doi.org/10.1016/j.scitotenv.2021.149093.

Chen, H., Zeng, L., Wang, D., Zhou, Y., Yang, X., 2020. Recent advances in nitrous oxide production and mitigation in wastewater treatment. Water. Res. 184. https://doi.org/10.1016/j.watres.2020.116168.

Ding, X., Zhao, J., Hu, B., Chen, Y., Ge, G., Li, X., Wang, S., Gao, K., Tian, X., 2016. Mathematical modeling of nitrous oxide production in an anaerobic/oxic/anoxic

process. Bioresour. Technol. 222, 39–48. https://doi.org/10.1016/j.biortech.2016.09.092.
Duan, H., Ye, L., Erler, D., Ni, B.J., Yuan, Z., 2017. Quantifying nitrous oxide production pathways in wastewater treatment systems using isotope technology – a critical review. Water. Res. 122, 96–113. https://doi.org/10.1016/j.watres.2017.05.054.
Harris, E., Joss, A., Emmenegger, L., Kipf, M., Wolf, B., Mohn, J., Wunderlin, P., 2015. Isotopic evidence for nitrous oxide production pathways in a partial nitritation-anammox reactor. Water. Res. 83, 258–270. https://doi.org/10.1016/j.watres.2015.06.040.
[IPCC, 2021. In: Masson-Delmotte, V., Zhai, P., Pirani, A., Connors, S.L., Péan, C., Berger, S., Caud, N., Chen, Y. (Eds.), Climate Change 2021: The Physical Science Basis. Contribution of Working Group I to the Sixth Assessment Report of the Intergovernmental Panel on Climate Change. Cambridge, United Kingdom and New York, NY, USA. Cambridge University Press. https://doi.org/10.1017/9781009157896 [.
Kampschreur, M.J., van der Star, W.R.L., Wielders, H.A., Mulder, J.W., Jetten, M.S.M., van Loosdrecht, M.C.M., 2008. Dynamics of nitric oxide and nitrous oxide emissions during full-scale reject water treatment. Water. Res. 42, 812–826. https://doi.org/10.1016/j.watres.2007.08.022.
Khalil, M., AlSayed, A., Liu, Y., Vanrolleghem, P.A., 2023. Machine learning for modeling N2O emissions from wastewater treatment plants: Aligning model performance, complexity, and interpretability. Water. Res. 245, 120667. https://doi.org/10.1016/j.watres.2023.120667.
Law, Y., Ni, B.J., Lant, P., Yuan, Z., 2012. N2O production rate of an enriched ammonia-oxidising bacteria culture exponentially correlates to its ammonia oxidation rate. Water. Res. 46, 3409–3419. https://doi.org/10.1016/j.watres.2012.03.043.
Longo, S., Frison, N., Renzi, D., Fatone, F., Hospido, A., 2017. Is SCENA a good approach for side-stream integrated treatment from an environmental and economic point of view? Water. Res. 125, 478–489. https://doi.org/10.1016/j.watres.2017.09.006.
Lu, L., Guest, J.S., Peters, C.A., Zhu, X., Rau, G.H., Ren, Z.J., 2018. Wastewater treatment for carbon capture and utilization. Nat. Sustain. 1, 750–758. https://doi.org/10.1038/s41893-018-0187-9.
Lv, Y., Zhang, S., Xie, K., Liu, G., Qiu, L., Liu, Y., Zhang, Y., 2022. Establishment of nitrous oxide (N2O) dynamics model based on ASM3 model during biological nitrogen removal via nitrification. Environ. Technol. 43, 1170–1180. https://doi.org/10.1080/09593330.2020.1822447.
Mampaey, K.E., Spérandio, M., van Loosdrecht, M.C.M., Volcke, E.I.P., 2019. Dynamic simulation of N2O emissions from a full-scale partial nitritation reactor. Biochem. Eng. J. 152, 107356. https://doi.org/10.1016/j.bej.2019.107356.
Ni, B.J., Yuan, Z., 2015. Recent advances in mathematical modeling of nitrous oxides emissions from wastewater treatment processes. Water. Res. 87, 336–346. https://doi.org/10.1016/j.watres.2015.09.049.
Peng, L., Ni, B.J., Law, Y., Yuan, Z., 2016. Modeling N_2O production by ammonia oxidizing bacteria at varying inorganic carbon concentrations by coupling the catabolic and anabolic processes. Chem. Eng. Sci. 144, 386–394. https://doi.org/10.1016/j.ces.2016.01.033.
Peng, L., Ni, B.J., Ye, L., Yuan, Z., 2015. N_2O production by ammonia oxidizing bacteria in an enriched nitrifying sludge linearly depends on inorganic carbon concentration. Water. Res. 74, 58–66. https://doi.org/10.1016/j.watres.2015.02.003.
Pocquet, M., Wu, Z., Queinnec, I., Spérandio, M., 2016. A two pathway model for N2O emissions by ammonium oxidizing bacteria supported by the NO/N_2O variation. Water. Res. 88, 948–959. https://doi.org/10.1016/j.watres.2015.11.029.
Schleussner, C.F., Rogelj, J., Schaeffer, M., Lissner, T., Licker, R., Fischer, E.M., Knutti, R., Levermann, A., Frieler, K., Hare, W., 2016. Science and policy characteristics of the Paris Agreement temperature goal. Nat. Clim. Chang. 6, 827–835. https://doi.org/10.1038/nclimate3096.
Schreiber, F., Wunderlin, P., Udert, K.M., Wells, G.F., 2012. Nitric oxide and nitrous oxide turnover in natural and engineered microbial communities: Biological pathways, chemical reactions, and novel technologies. Front. Microbiol. 3, 1–24. https://doi.org/10.3389/fmicb.2012.00372.
Soler-Jofra, A., Stevens, B., Hoekstra, M., Picioreanu, C., Sorokin, D., van Loosdrecht, M. C.M., Pérez, J., 2016. Importance of abiotic hydroxylamine conversion on nitrous oxide emissions during nitritation of reject water. Chem. Eng. J. 287, 720–726. https://doi.org/10.1016/j.cej.2015.11.073.
Solís, B., Guisasola, A., Pijuan, M., Corominas, L., Baeza, J.A., 2022. Systematic calibration of N2O emissions from a full-scale WWTP including a tracer test and a global sensitivity approach. Chem. Eng. J. 435, 134733. https://doi.org/10.1016/j.cej.2022.134733.
Su, Q., Domingo-Félez, C., Jensen, M.M., Smets, B.F., 2019. Abiotic Nitrous Oxide (N 2 O) Production Is Strongly pH Dependent, but Contributes Little to Overall N 2 O Emissions in Biological Nitrogen Removal Systems. Environ. Sci. Technol. 53, 3508–3516. https://doi.org/10.1021/acs.est.8b06193.
Terada, A., Sugawara, S., Hojo, K., Takeuchi, Y., Riya, S., Harper, W.F., Yamamoto, T., Kuroiwa, M., Isobe, K., Katsuyama, C., Suwa, Y., Koba, K., Hosomi, M., 2017. Hybrid Nitrous Oxide Production from a Partial Nitrifying Bioreactor: Hydroxylamine Interactions with Nitrite. Environ. Sci. Technol. 51, 2748–2756. https://doi.org/10.1021/acs.est.6b05521.
Vasilaki, V., Massara, T.M., Stanchev, P., Fatone, F., Katsou, E., 2019. A decade of nitrous oxide (N2O) monitoring in full-scale wastewater treatment processes: A critical review. Water. Res. 161, 392–412. https://doi.org/10.1016/j.watres.2019.04.022.
Wunderlin, P., Mohn, J., Joss, A., Emmenegger, L., Siegrist, H., 2012. Mechanisms of N2O production in biological wastewater treatment under nitrifying and denitrifying conditions. Water. Res. 46, 1027–1037. https://doi.org/10.1016/j.watres.2011.11.080.
Zhao, J., Lei, S., Cheng, G., Zhang, J., Shi, B., Xie, S., Zhao, J., 2022. Comparison of inhibitory roles on nitrite-oxidizing bacteria by hydroxylamine and hydrazine during the establishment of partial nitrification. Bioresour. Technol. 355, 127271. https://doi.org/10.1016/j.biortech.2022.127271.